# Reactions of Laser-Ablated Mg, Ca, Sr, and Ba Atoms with Hydrogen Cyanide in Excess Argon. Matrix Infrared Spectra and Density Functional Calculations on Novel Isocyanide Products

**Dominick V. Lanzisera and Lester Andrews***

*Department of Chemistry, University of Virginia, Charlottesville, Virginia 22901*

*Received: June 30, 1997; In Final Form: September 29, 1997*[⊗]

Laser-ablated alkaline earth metal atoms reacting with hydrogen cyanide in the presence of excess argon produce matrix-isolated linear metal isocyanides, MNC, but no noticeable amount of the corresponding cyanide isomer, MCN. Supplemental experiments with DCN show that, unlike the corresponding beryllium reactions, no products containing hydrogen are formed. Experiments with isotopically enriched $H^{13}CN$ yield $MN^{13}C$ shifted 40 $cm^{-1}$ from $MN^{12}C$ in the C≡N stretching frequency, with the isotopic shift virtually independent of the alkaline earth metal. As the mass of the group 2 metal increases, the C≡N frequency decreases and the absorption becomes broader, the latter feature indicating a decreasingly rigid linear geometry. The lack of MCN indicates that the products form via attack of the energetic metal on the nitrogen atom, instead of through insertion into the C−H bond.

## Introduction

There has been a good deal of recent interest in the spectroscopy of alkaline earth cyanides. In 1986, a series of unidentified microwave spectral lines from the circumstellar envelope of the star IRC + 10216 did not match those of known molecules,[1] and it was only in 1993 that Kawaguchi et al.[2] reproduced these lines in the laboratory and assigned them to magnesium isocyanide, MgNC. Rotational spectra[3] of the isotopic species, $^{25}$MgNC and $^{26}$MgNC, and subsequent detection[4] of these radicals in the star IRC+10216 confirmed this assignment. Subsequently, the less abundant MgCN isomer was detected both in the star[5] and in the laboratory.[6]

Prior to their discovery in space, Bauschlicher et al. performed ab initio calculations on MgNC, MgCN, and other alkaline earth cyanides and isocyanides at the SCF and CI levels.[7] Unlike the alkali metal counterparts, which are essentially T-shaped, the group 2 radicals were shown to be linear and of the forms MNC and MCN, where M is the alkaline earth metal. In each case, the isocyanide was the more stable isomer. Rotational spectra of MgNC confirmed the predicted linear structure.[8]

Experimental work for the other alkaline earth monocyanides is less complete. Dagdigian and co-workers[9,10] first observed the monocyanides of Ca, Sr, and Ba, and these products were later interpreted to be isocyanides. Low-resolution LIF spectra of CaNC and SrNC gave evidence for linear structures,[11,12] and further experiments confirmed this geometry for CaNC.[13,14] The generally accepted representation of these radicals has a mainly ionic bond between $M^+$ and $NC^-$, with the unpaired electron residing primarily on M.

Matrix isolation FTIR studies of the reactions of laser-ablated beryllium atoms with hydrogen cyanide provide the only spectroscopic evidence of the vibrational frequencies of alkaline earth cyanides and monocyanides thus far.[15] Density functional theory (DFT) calculations on the products of this reaction helped determine the identification of the cyanides, HBeCN and BeCN, and the isocyanides, HBeNC and BeNC. BeNC was the dominant product, and its peak intensity in the signature C≡N stretching region was much stronger than the corresponding BeCN band. The DFT calculations predicted that the oscillator strength of the former should be significantly greater, but the vast peak intensity difference suggested that BeNC is more stable than BeCN, an observation that Bauschlicher et al. predicted.[7] The frequency of the C≡N stretching vibration of the cyanides was significantly higher than that of the isocyanides, which is consistent with observations made in studies of cyanides and isocyanides of boron[16,17] and the other group 13 elements.[18]

In this paper, we report FTIR spectra of the heavier group 2 isocyanides, MgNC, CaNC, SrNC, and BaNC. DFT calculations of all of these products, as well as of the corresponding MCN radicals, are presented and combined with more sophisticated calculations to help suggest reasons for the absence of MCN absorptions. Comparisons of the C≡N stretching frequencies among the various alkaline earth monocyanides will be made as well as a discussion of the reaction mechanism.

## Experimental Section

The experimental apparatus has been described previously.[15−16,19] Mixtures of 0.3% HCN or $H^{13}CN$ in Ar co-deposited at 3 mmol/h for 2 h onto a 6−10 K cesium iodide window react with metal atoms ablated from a target source rotating at 1 rpm. The fundamental 1064 nm beam of a Nd:YAG laser (Spectra Physics DCR-11) operating at 10 Hz and focused with a f.l. = +10 cm lens ablate the target using 10−20 mJ per 10 ns pulse. The metal samples employed were $^{n}$Mg (Fisher), $^{26}$Mg (96%, Oak Ridge National Laboratory), Ca (Alfa, ingot, 99%), Sr (Alfa, ingot, 99%), and Ba (Alfa, rod, 99.5%). The procedure for preparing HCN is described in detail elsewhere.[15,16,20] For $H^{13}CN$, we added concentrated HCl to $K^{13}CN$ (Cambridge Isotope Laboratories) and obtained a $H^{13}CN$:$H^{12}CN$ ratio of approximately 2:1 for the Sr and Ba experiments and greater than 4:1 for the Mg and Ca experiments. Following deposition infrared spectra were collected on a Nicolet 550 or Nicolet 750 Fourier transform infrared (FTIR) spectrometer from 4000 to 400 $cm^{-1}$ using a liquid nitrogen cooled MCTB detector and KBr beam splitter with a resolution of 0.5 $cm^{-1}$ with an accuracy of 0.2 $cm^{-1}$. After sample deposition, annealing to 15 K followed by broadband (240−580 nm) mercury arc photolysis

[⊗] Abstract published in *Advance ACS Abstracts,* December 1, 1997.

S1089-5639(97)02098-7 CCC: $14.00 

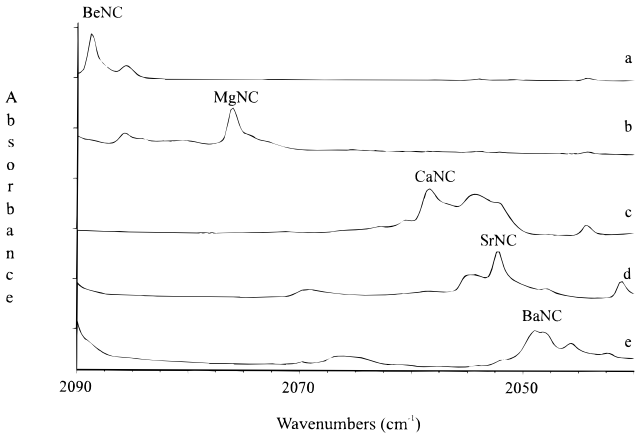


**Figure 1.** Matrix infrared spectra in the 2090−2040 cm$^{-1}$ C≡N stretching region following co-deposition of pulsed-laser ablated alkaline earth metal atoms with Ar/H$^{12}$CN (300/1) samples on a CsI window at 6−10 K: (a) Be, (b) $^{n}$Mg, (c) Ca, (d) Sr, and (e) Ba.

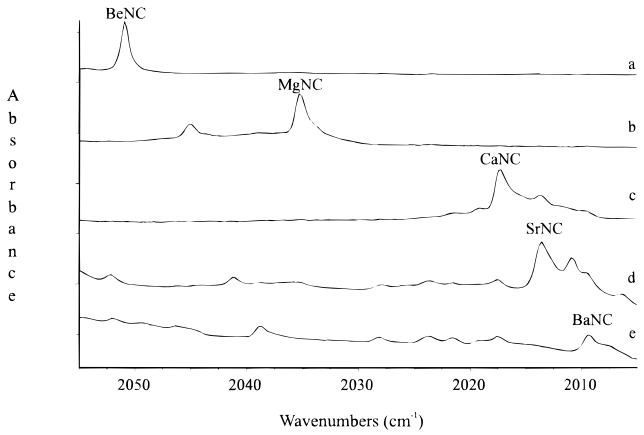


**Figure 2.** Matrix infrared spectra in the 2055−2005 cm$^{-1}$ C≡N stretching region following co-deposition of pulsed-laser ablated alkaline earth metal atoms with Ar/H$^{13}$CN (300/1) samples on a CsI window at 6−10 K: (a) Be, (b) $^{n}$Mg, (c) Ca, (d) Sr, and (e) Ba.

(Philips 175 W, globe removed) altered the features of the FTIR spectra, as did further annealings to 25 and 35 K. Far-infrared spectra were recorded from 600 to 200 cm$^{-1}$ using a DTGS detector and solid-state beam splitter at 1 cm$^{-1}$ resolution and accuracy. It must be noted that the MCTB detector is 30 times more sensitive than the DTGS detector and that far-infrared FTIR spectra are much more sensitive to mechanical noise.

Density functional theory calculations were performed on potential product molecules using the Gaussian 94 program package.[21] These calculations used effective core potentials for the M atoms. The basis sets for the light atoms were 6-311G with one single first polarization function (6-311G*),[22,23] and the LANL2DZ basis sets[24−26] were used for the group 2 atoms. For MgNC, CaNC, and SrNC, DFT calculations using the BP86 functional[27,28] provide the best vibrational frequencies. This method did not work for BaCN, BaNC, and SrCN, and the simple unrestricted Hartree−Fock (HF) method was employed for these species. Because the BP86 calculations did not converge for BaNC, MP2 calculations[29−31] were employed to improve upon the HF method and yield more accurate vibrational frequency predictions. The geometry optimizations converged via the Berny optimization algorithm.[21,32]

## Results

Matrix infrared spectra for the C≡N stretching region for the products of M + HCN (M = Mg, Ca, Sr, Ba) reactions are reported for both $^{12}$C and $^{13}$C products in Figures 1 and 2, respectively. In addition, spectra from beryllium−hydrogen cyanide reactions[15] are presented for comparison. The spectra are not on a common scale and are instead normalized to each other because the higher yield product peaks of certain experiments, such as those of beryllium, would otherwise obscure the lower yield product peaks of other experiments, such as those of barium. The different ablation characteristics and reactivities of the metals result in the various observed yields. Figure 3 presents lower frequency spectra for magnesium compounds for three isotopic combinations with all bands on a common scale. In Figures 1 and 2, only $^{n}$Mg spectra are presented, as there is no observable isotopic shift in any of the C≡N peaks in the $^{26}$Mg spectra. All pertinent absorption bands, along with their respective photolysis and annealing behaviors, are presented in Table 1. Of the hydrides,[33−35] only a trace of MgH was detected. With the exception of the beryllium products,[15] no alkaline earth cyanide products contain hydrogen atoms, as determined by separate experiments with DCN.

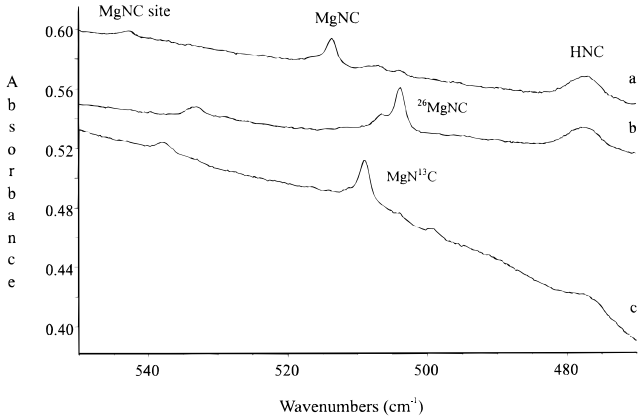


**Figure 3.** Matrix infrared spectra in the 550−470 cm$^{-1}$ Mg−N stretching region following co-deposition of pulsed-laser ablated Mg atoms with Ar/HCN (300/1) samples on a CsI window at 6−7 K: (a) $^{n}$Mg + H$^{12}$CN, (b) $^{26}$Mg + H$^{12}$CN, and (c) $^{n}$Mg + H$^{13}$CN.

**TABLE 1: Observed Frequencies (cm$^{-1}$) for Products from Reactions of Hydrogen Cyanide with Group 2 Elements**

| M + H$^{12}$CN | M + H$^{13}$CN | photolysis[a] | annealing[b] | identity |
|---|---|---|---|---|
| 2183.1 | 2134.6 | +35 | −35 | BeCN |
| 2088.7 | 2050.8 | −45 | −5 | BeNC |
| 2085.7 | 2045.0 | +95 | +60 | $^{24}$MgNC site |
| 2085.7 | 2045.0 | +95 | +60 | $^{26}$MgNC site |
| 2076.1 | 2035.2 | −35 | +45 | $^{24}$MgNC |
| 2076.1 | 2035.2 | −35 | +45 | $^{26}$MgNC |
| 1420.1 | 1420.1 | 0 | +15 | MgH |
| 542.9 | 538.0 | +95 | +60 | $^{24}$MgNC site |
| 533.2 | | +95 | +60 | $^{26}$MgNC site |
| 513.7 | 509.0 | −35 | +45 | $^{24}$MgNC |
| 503.9 | | −35 | +45 | $^{26}$MgNC |
| 2058.4 | 2017.3 | −5 | +20 | CaNC |
| 2052.3 | 2013.6 | −15 | +20 | SrNC |
| 2048.9 | 2009.3 | +150 | −20 | BaNC |
| 2154.0 | 2017.5 | | | $(CN)_2$ |
| 2044.3 | 2002.0 | | | CN |
| 2027.8 | 1984.9 | | | HNC |
| 477.8 | 477.3 | | | HNC |

[a] Percent increase or decrease on 30 min photolysis. [b] Percent increase or decrease on annealing to 25 K.

**Mg + HCN.** Figure 1b represents the spectrum of reactions of $^{n}$Mg with H$^{12}$CN, while Figure 2b gives the corresponding H$^{13}$CN spectrum, both following 2 h of deposition. The main band in Figure 1b at 2076.1 cm$^{-1}$ has a satellite at 2085.7 cm$^{-1}$. On photolysis, the intensity of the larger peak decreases in intensity while splitting into two bands, and the satellite intensity

increases. A similar absorption profile is present in Figure 2. Both bands shift approximately 40 $cm^{-1}$ on carbon-13 substitution. These absorptions represent the only product peaks in the C≡N stretching region of the spectrum as there are no new bands above 2100 $cm^{-1}$.

In experiments investigating MgCCH, which is isoelectronic with MgCN and MgNC, the Mg−C single bond stretching frequency was determined to be 500 ± 5 $cm^{-1}$ in the gas phase[36] and 491.8 $cm^{-1}$ in an argon matrix.[37] Because of the similarity to this molecule, the same vibrational stretching absorption in MgCN should appear close to this frequency. On the basis of other studies of monocyanides and isocyanides in argon matrixes, the Mg−N stretching absorption in MgNC should appear somewhat higher in frequency than the MgCN band.[15−18] In Figure 3, two new sets of bands may be observed in addition to the HNC bending mode absorptions. The stronger of the two peaks is at 513.7 $cm^{-1}$ for natural isotopes. Unlike the bands in the C≡N stretching region, this absorption exhibits a significant magnesium isotopic shift to 503.9 $cm^{-1}$ with $^{26}Mg$, as can be seen in Figure 3b. Because $^{n}Mg$ has approximately 10% each of $^{25}Mg$ and $^{26}Mg$, a trace of the $^{26}Mg$ absorption can be seen, as well as a $^{25}Mg$ band at 507.5 $cm^{-1}$. This latter band can also be seen as a shoulder in Figure 3b because the $^{26}Mg$ sample possesses a trace of $^{25}Mg$ as well. The carbon-13 shift of this band, determined by comparing parts a and c of Figure 3, is 4.7 $cm^{-1}$, indicating a vibrational mode with carbon influence in addition to magnesium motion. This peak decreases in intensity and splits into two bands on photolysis, thereby tracking with the stronger, sharper absorptions in Figures 1b and 2b.

The other peak in this lower frequency region at 542.9 $cm^{-1}$ has a 9.7 $cm^{-1}$ magnesium-26 shift and a 4.9 $cm^{-1}$ carbon-13 shift. This absorption tracks well with the weaker band observed in the C≡N region in Figures 1b and 2b. Noteworthy is that the isotopic shifts for the 2076.1/513.7 $cm^{-1}$ and 2085.7/542.9 $cm^{-1}$ sets of peaks are similar. All other magnesium absorptions observed in these experiments result from MgH at 1422.1 $cm^{-1}$ and from magnesium oxides,[38] caused by unavoidable oxidation on the target surface.

**Ca + HCN.** Figures 1c and 2c present infrared spectra of the products of reactions of Ca with $H^{12}CN$ and $H^{13}CN$, respectively. The dominant absorptions are at 2058.4 and 2017.3 $cm^{-1}$ for the two isotopic molecules, and both bands decrease by a small amount on photolysis and increase 20% on annealing. As with magnesium, no new bands above 2100 $cm^{-1}$ were observed. Very weak calcium oxide absorptions[39] were observed, and these arise from surface oxides on the calcium target. A weak band at 403 $cm^{-1}$ at the MCTB detector limit is associated with the 2058.4 $cm^{-1}$ band on photolysis and annealing. Using the solid-state beam splitter gave the same 403 ± 1 $cm^{-1}$ band in the far-infrared region with increased noise (Figure 4a). This band shifted to 399 ± 1 $cm^{-1}$ with $H^{13}CN$ (Figure 4b) following the shift of the 2058.4 $cm^{-1}$ band to 2017.3 $cm^{-1}$ observed in the mid- IR with the KBr beam splitter.

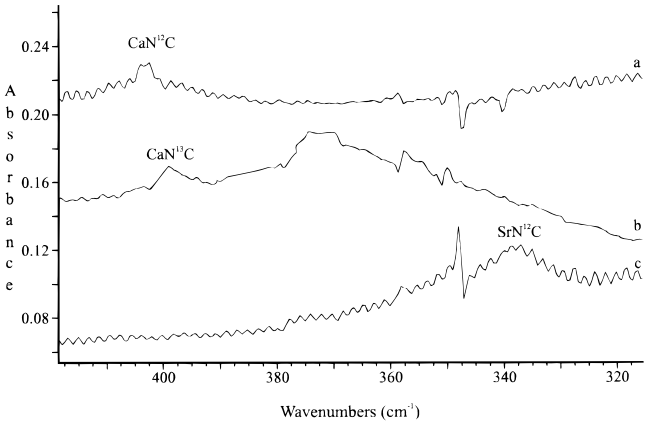


**Figure 4.** Matrix far-infrared spectra in the 420−315 $cm^{-1}$ region following co-deposition of pulsed-laser ablated Ca or Sr atoms with Ar/HCN (100/1) samples on a CsI window at 10 K: (a) Ca + $H^{12}CN$, (b) Ca + $H^{13}CN$, and (c) Sr + $H^{12}CN$.

**Sr + HCN.** Figures 1d and 2d present product spectra of strontium−hydrogen cyanide reactions. The softness of the Sr and Ba targets required ablation at relatively low laser pulse energies, resulting in smaller yields for these experiments. In the strontium experiments, a sharp band emerges at 2052.3 and 2013.6 $cm^{-1}$ for $H^{12}CN$ and $H^{13}CN$, respectively with matrix sites to the blue for the former and to the red for the latter; as with the other metals, weak oxide absorptions[39] were present in the spectra. Far-infrared spectra in these experiments revealed associated bands at 338 ± 2 $cm^{-1}$ for $H^{12}CN$ (Figure 4c) and 336 ± 2 $cm^{-1}$ for $H^{13}CN$.

**Ba + HCN.** Barium−hydrogen cyanide product spectra are presented in Figures 1e and 2e. As with Ca and Sr, satellite absorptions accompany the main peaks at 2048.9 $cm^{-1}$ and 2009.3 $cm^{-1}$, and the frequencies and band shapes of these satellites vary with each experiment. The "main" absorption grows enormously on photolysis and decreases somewhat on annealing. Similar to the other group 2 experiments, no bands above 2100 $cm^{-1}$ were observed. These experiments failed to give a far-infrared product absorption.

**Be + HCN.** Figures 1a and 2a present spectra of beryllium−hydrogen cyanide reactions.[15] Although there are lower frequency absorptions near 800−900 $cm^{-1}$, only absorptions between 2000 and 2100 $cm^{-1}$ are shown. Unlike the other alkaline earth experiments, reactions of Be with HCN generated products with absorptions above 2100 $cm^{-1}$, and one of these products, BeCN, is listed in Table 1, along with BeNC.

**Calculations.** BP86 calculations with the LANL2DZ basis sets and effective core potential on the M atom and the 6-311G* basis sets on the C and N atoms are presented in Table 2 for several possible group 2 monocyanides and isocyanides. Ge-

**TABLE 2: BP86 Calculations for Products and Other Species From Reactions of MCN and MNC, Where M = Be, Mg, Ca, or Sr[a]**

| product | energy (au) | bond lengths (Å)[b] | frequencies in $cm^{-1}$ (intensities in km $mol^{-1}$)[c] |
|---|---|---|---|
| BeNC | −107.542 17 | $r_{BeN}$ = 1.57; $r_{CN}$ = 1.19 | 2058.0(367), 883.2(137), 160.1(0), 160.1(0) |
| BeCN | −107.540 34 | $r_{BeC}$ = 1.69; $r_{CN}$ = 1.17 | 2195.0(81), 782.3(112), 242.4(4), 242.4(4) |
| MgNC | −93.685 50 | $r_{MgN}$ = 1.97; $r_{CN}$ = 1.19 | 2056.0(204), 499.7(77), 104.2(0), 104.2(0) |
| MgCN | −93.684 85 | $r_{MgC}$ = 2.10; $r_{CN}$ = 1.17 | 2160.5(30), 434.8(68), 165.5(1), 165.5(1) |
| CaNC | −129.428 30 | $r_{CaN}$ = 2.32; $r_{CN}$ = 1.19 | 2066.9(136), 392.3(60), 101.6(0), 101.6(0) |
| CaCN | −129.426 49 | $r_{CaC}$ = 2.47; $r_{CN}$ = 1.17 | 2149.9(16), 351.8(61), 144.2(0), 144.2(0) |
| SrNC | −123.320 75 | $r_{SrN}$ = 2.46; $r_{CN}$ = 1.19 | 2068.1(112), 322.7(49), 79.1(0), 79.1(0) |

[a] The LANL2DZ basis set was used for each M atom, and the 6-311G* basis set was used for C and N. [b] All products are linear molecules. [c] For the major stable isotope.

**TABLE 3: Experimental Frequencies and BP86 Calculations on Isomers of $Mg(CN)_n$, Where $n = 1-2$**

| | | calculations | | | | |
|---|---|---|---|---|---|---|
| Mg/C isotopes[a] | exptl | MgNC | MgCN | $Mg(CN)_2$ | Mg(CN)-(NC) | $Mg(NC)_2$ |
| 24/12 | 2076.1 | 2056.0 | 2160.5 | 2178.6[b] | 2060.0[b] | 2059.3[b] |
| 26/12 | 2076.1 | 2055.9 | 2160.4 | 2178.5[b] | 2060.0[b] | 2059.2[b] |
| 24/13 | 2035.2 | 2014.9 | 2113.2 | 2130.6[b] | 2019.3[b] | 2018.6[b] |
| 24/12 | 513.7 | 499.7 | 434.8 | 581.7 | 627.7 | 655.3 |
| 26/12 | 503.9 | 489.6 | 426.0 | 566.2 | 611.2 | 637.8 |
| 24/13 | 509.0 | 494.7 | 431.3 | 578.9 | 623.7 | 650.6 |

[a] Mass numbers of magnesium/carbon isotopes. [b] More intense of two C≡N vibrational modes.

ometry optimizations would not converge for SrCN, BaNC, and BaCN. Although more inclusive basis sets were available for Be and Mg, all used the LANL2DZ sets for comparison with the calcium and strontium calculations. The BP86 method tends to overestimate bond lengths but predicts vibrational frequencies very accurately.[40] All species are calculated to be linear, with the isocyanide more stable than the cyanide for each alkaline earth element. Similar to calculations of cyanide products in other experiments, the M−N bonds of MNC are shorter than the corresponding M−C bonds of MCN, while the situation is reversed for the respective C≡N bonds. This leads to higher M−X (X = C, N) stretching frequencies and lower C≡N frequencies for the isocyanide compared to the cyanide. All frequencies calculated here were harmonic values.

## Discussion

**MgNC.** The FTIR spectra in Figures 1−3 appear to indicate two sets of product bands, one large set which decreases in intensity on photolysis and a smaller set which increases in intensity. The DFT calculations in Table 2 predict a 137 $cm^{-1}$ separation between MgCN and MgNC, which seems to indicate that the bands at 2076.1 and 2085.7 $cm^{-1}$ are matrix sites of the isocyanide. Consistent with this interpretation is that, in the other cyanide/isocyanide systems studied, all cyanide absorptions appear above 2100 $cm^{-1}$.[15−18] These calculations also predict that the C≡N stretching vibration of MgCN has a much weaker oscillator strength than that of MgNC.

Another possibility is that one of these two bands is MgNC, while the other represents $Mg(NC)_2$ or Mg(CN)(NC). Calculations by Kapp and Schleyer[41] predict all three isomers of $Mg(CN)_2$, including Mg(CN)(NC) and $Mg(NC)_2$, to be within 1 kcal $mol^{-1}$ of each other in energy. Frequency calculations on these molecules and MgNC, presented in Table 3 with the experimental frequencies, show that the Mg−N stretching modes of the dicyanide isomers have much larger magnesium isotopic shifts than those observed in the experiment. The magnesium-26 shifts of both bands in Figure 3 are nearly the same and indicate similar magnesium involvement in the mode. The magnesium motion in any isomer of $Mg(CN)_2$ for a Mg−C or Mg−N stretch is antisymmetric and substantially different from the magnesium motion in MgNC or MgCN. Thus, neither of these bands in the spectra denotes a dicyanide. That no dicyanide isomers are observed is not surprising considering the low concentration of HCN in Ar used in these experiments.

As with the beryllium cyanides, DFT/BP86 calculations on MgNC and MgCN help explain the spectra accurately. These frequency calculations are presented in Table 4 as well as previous calculations by other groups. Energies are not listed, but MgCN is calculated to be less stable than MgNC by only 0.3 kcal $mol^{-1}$, which is reasonable given higher level predictions of 1.5−3.9 kcal $mol^{-1}$ energy difference.[7,42−44] Nevertheless, the C≡N stretching vibrational frequency of MgCN is calculated to be about 100 $cm^{-1}$ higher than that of MgNC, which is consistent with other MCN/MNC systems and suggests that, despite the apparently small energy difference between the two isomers, the lack of appropriate bands above 2100 $cm^{-1}$ suggests that no observable amount of MgCN is produced in these experiments. Note also that the 513.7 $cm^{-1}$ band is much closer to the calculated Mg−N stretching mode than the calculated Mg−C mode. Thus, the two bands observed in Figures 1-3 are, therefore, due to MgNC in two different matrix environments. The similar isotopic shifting behavior of these bands is further evidence that these bands are of the same species. The DFT/BP86 calculations predict the MgNC frequencies with excellent accuracy, as Table 4 shows. Any matrix conformation which distorts MgNC from linearity could result in the minor matrix sites at 2085.7 and 542.9 $cm^{-1}$ (for natural isotopes).

**TABLE 4: Observed and Calculated Frequencies ($cm^{-1}$) for MgNC and MgCN**

| product | exptl | BP86[a] | HF[a] | MP2[b] | corrected HF[c] | RHF[d] |
|---|---|---|---|---|---|---|
| $^{24}MgN^{12}C$ | 2076.1 | 2056.0 | 2315.0 | 2081 | 2082.8 | 2319 |
| $^{26}MgN^{12}C$ | 2076.1 | 2055.9 | 2315.0 | | | |
| $^{24}MgN^{13}C$ | 2035.2 | 2014.9 | 2268.4 | | | |
| $^{24}MgN^{12}C$ | 513.7 | 499.7 | 534.4 | 524 | 493.0 | 556 |
| $^{26}MgN^{12}C$ | 503.9 | 489.6 | 523.6 | | | |
| $^{24}MgN^{13}C$ | 509.0 | 494.7 | 529.2 | | | |
| $^{24}Mg^{12}CN$ | | 2160.5 | 2335.0 | 3598 | 2218.5 | 2469 |
| $^{26}Mg^{12}CN$ | | 2160.4 | 2335.0 | | | |
| $^{24}Mg^{13}CN$ | | 2113.2 | 2284.2 | | | |
| $^{24}Mg^{12}CN$ | | 434.8 | 501.2 | 473 | 423.2 | 474 |
| $^{26}Mg^{12}CN$ | | 426.0 | 491.1 | | | |
| $^{24}Mg^{13}CN$ | | 431.3 | 497.1 | | | |

[a] This work (see text). [b] From ref 41 with 6-31G* basis sets. [c] From ref 42 with 6-31G* basis sets. [d] From ref 43 with TZ2P basis sets.

**TABLE 5: Experimental and Calculated Frequencies ($cm^{-1}$) and Carbon-13 Isotopic Ratios for CaNC**

| | exptl | BP86 | HF |
|---|---|---|---|
| $CaN^{12}C$ | 2058.4 | 2066.9 | 2325.5 |
| $CaN^{13}C$ | 2017.3 | 2025.1 | 2278.2 |
| ratio[a] | 1.02037 | 1.02064 | 1.02076 |
| $CaN^{12}C$ | 403 ± 1 | 392 | 426 |
| $CaN^{13}C$ | 399 ± 1 | 388 | 421 |
| ratio[a] | 1.0100 | 1.0103 | 1.0119 |

[a] Carbon-12 frequency divided by carbon-13 frequency.

**CaNC.** Analysis of the magnesium spectra makes identification of the products for the other alkaline earth reaction spectra reasonably straightforward. Although there appear to be a few bands in the 2050−2060 $cm^{-1}$ range in Figure 1c, these peaks are most likely due to different matrix site positions of CaNC. The 41.1 $cm^{-1}$ carbon-13 shift is consistent with the MNC isomer, while the MCN isomer isotopic shift is typically larger.[18] Table 5 lists the observed and calculated frequencies for both isotopic forms of CaNC. Although the HF frequencies are characteristically too high, the carbon isotopic ratios are in excellent agreement with those of the matrix spectra.

The calculations also indicate that the Ca−N stretch of CaNC may be observable at the low end of the experimental frequency range, and the 403 $cm^{-1}$ band associated with the 2058.4 $cm^{-1}$ band on annealing and photolysis is assigned to this mode. By assuming that the $CN^-$ group behaves as a pseudohalide with properties at the midpoint between those of $F^-$ and $Cl^-$, Douay and Bernath predicted that the Ca−N stretch in CaNC should appear at 464 $cm^{-1}$, given those of CaF (581 $cm^{-1}$) and CaCl (367 $cm^{-1}$).[12] Similarly, based on the frequency of CaNNN (396 $cm^{-1}$), they predicted a CaNC stretching frequency of 449

**TABLE 6: Experimental and Calculated Frequencies ($cm^{-1}$) and Carbon-13 Isotopic Ratios for SrNC**

| | exptl | BP86 | HF |
|---|---|---|---|
| $SrN^{12}C$ | 2052.3 | 2068.1 | 2328.0 |
| $SrN^{13}C$ | 2013.6 | 2026.0 | 2280.3 |
| ratio[a] | 1.01922 | 1.02078 | 1.02092 |
| $SrN^{12}C$ | $338 \pm 2$ | 323 | 350 |
| $SrN^{13}C$ | $336 \pm 2$ | 318 | 346 |
| ratio[a] | 1.0060 | 1.0157 | 1.0116 |

[a] Carbon-12 frequency divided by carbon-13 frequency.

$cm^{-1}$. Calculated frequencies listed in Table 5 are in very good agreement with the observed C≡N stretching frequency and predict a Ca−N stretching frequency at 392 $cm^{-1}$ for natural isotopes, which is near with the observed 403 $cm^{-1}$ band. The calculated carbon-13 shift, 4 $cm^{-1}$, is also in very good agreement with the 4 $cm^{-1}$ observed shift. Interestingly, in LIF spectra, Douay and Bernath observed 392 and 370 $cm^{-1}$ intervals, which were thought to be inconsistent with the Ca−N stretching mode,[12] but these intervals may in fact be due to such a vibrational spacing.

**SrNC.** With Figures 1d and 2d, two trends established in the Be, Mg, and Ca spectra are further reinforced. The first is the tendency of broader matrix site distribution of MNC with increasing atomic mass of M. The main SrNC peak at 2052.3 $cm^{-1}$ has some satellites to the red, with the difference in site structure between Figures 1d and 2d again determined by the specific deposition conditions. This trend toward broader and less definitive absorptions of the C≡N stretch may be explained by the increasing "floppy" nature of these isocyanides as the size of M increases.[7] Despite this characteristic for SrNC, no spectroscopic evidence for the linear SrCN radical was observed. Although no previous calculations on these molecules have been reported, using the HF method, the calculated energy difference between the two isomers (6.9 kcal $mol^{-1}$) is between those calculated for Ca (7.1 kcal/$mol^{-1}$) and Ba (6.9 kcal/$mol^{-1}$), both of which are in reasonable agreement with Bauschlicher et al.[7] Table 6 presents the frequency calculations for both carbon isotopes using the HF and BP86 methods. As with calcium, the HF calculations predict frequencies which are too high, but both methods predict carbon isotopic ratios only slightly greater than those observed.

The second trend observable in these alkaline earth isocyanides is the tendency for the C≡N stretching frequency to decrease with increasing atomic mass of M. Although the HF and BP86 calculations do not predict this trend, it is obvious from the spectra that it exists for both carbon isomers. Accordingly, the carbon-13 shift for MNC is virtually independent of M, with an average value of 39.6 $cm^{-1}$ and standard deviation of only 1.4 $cm^{-1}$. With group 13 isocyanides, this isotopic shift was slightly proportional to the mass of M, and the C≡N stretching frequencies, themselves, were virtually independent of the size of M. This difference is one of the distinguishing features between group 2 and group 13 cyanides and isocyanides.[18]

Far-infrared spectra revealed a new 338 $cm^{-1}$ band, which showed the same annealing and photolysis behavior as the 2052.3 $cm^{-1}$ band. The observed 338 $cm^{-1}$ band is in good agreement with the 323 $cm^{-1}$ prediction of DFT/BP86 calculations.

Douay and Bernath,[12] in a similar treatment as with CaNC, estimated a Sr−N stretch at 393 $cm^{-1}$ based on the SrF frequency of 502 $cm^{-1}$ and the SrCl frequency of 302 $cm^{-1}$. By using the SrNNN stretching frequency of 316 $cm^{-1}$ as a guide, they calculated a SrNC frequency at 377 $cm^{-1}$. Both these estimates were inconsistent with their LIF data, however. The present 338 $cm^{-1}$ observation and 323 $cm^{-1}$ calculations suggest that the former estimates are too high.

**TABLE 7: Experimental and Calculated Frequencies ($cm^{-1}$) and Carbon-13 Isotopic Ratios for BaNC**

| | exptl | MP2 | HF |
|---|---|---|---|
| $BaN^{12}C$ | 2048.9 | 2057.2 | 2329.9 |
| $BaN^{13}C$ | 2009.3 | 2015.3 | 2282.0 |
| ratio[a] | 1.01971 | 1.02079 | 1.02099 |

[a] Carbon-12 frequency divided by carbon-13 frequency.

**BaNC.** The weakest of all alkaline earth isocyanide bands belong to BaNC in Figures 1e and 2e. The softness of Ba made ablating the target at even modest laser intensity problematic and therefore did not allow for production of high-energy barium atoms. Nevertheless, peaks can be seen at 2048.9 and 2009.3 $cm^{-1}$ for $H^{12}CN$ and $H^{13}CN$, respectively, consistent with an isocyanide. These peaks grow a great deal on photolysis, suggesting that CN groups formed in the ablation process associate with previously isolated Ba atoms under these conditions. The trends discussed in the previous subsection regarding SrNC continue with BaNC. The frequency of the C≡N stretch is the smallest when the size of M is largest. The carbon-13 isotopic shift is also consistent with previous observations. The breadth of the absorptions suggests that BaNC is the most "floppy" of all group 2 isocyanides.

Hartree−Fock calculations and observed frequencies for BaNC, as well as calculations for BaCN, are presented in Table 7. BP86 calculations would not converge for either product, but using the MP2 ab initio method provided good results for BaNC and are also presented in Table 7. As with the other alkaline earth products, the HF calculations determine close carbon isotopic ratios despite overestimating the absolute frequencies. The MP2 results are closer to the observed values, but because such calculations would not converge for BaCN, we could not determine the energy difference of the isomers with this method. Using the HF results, we obtain an energy difference of 6.9 kcal $mol^{-1}$, which is close to that of Bauschlicher et al.[7] (7.4 kcal $mol^{-1}$) and the other alkaline earth cyanide energy calculations. The MP2 calculations predict a Ba−N stretching absorption at 295 $cm^{-1}$.

**Absence of MCN.** The most intriguing result of these experiments is the complete lack of evidence for the production of MCN. For MgCN and MgNC, Petrie's G2 calculations predicted an enthalpy difference of only 1.5 kcal $mol^{-1}$ between the two isomers, with the isocyanide unsurprisingly the more stable radical.[43] This value is consistent with the energy difference provided by Ishii et al.[44] and a bit lower than the 3.0 kcal $mol^{-1}$ value of Bauschlicher et al.[7] Because the G2 method is generally one of the most accurate methods for determination of heats of formation, the value of $\Delta H_f = 1.5$ kcal $mol^{-1}$ for the conversion of MgNC to MgCN is probably quite close to the actual value.

Kawaguchi et al.[2] proposed that MgNC forms in the star IRC + 10216 via the following mechanism:

$$Mg^+ + HCN \rightarrow MgNCH^+ + h\nu \quad (1)$$

$$MgNCH^+ + e^- \rightarrow MgNC + H \quad (2)$$

MgCN would be formed either via a similar reaction of $Mg^+$ with HNC or rearrangement of MgNC. The observed HCN/HNC ratio is greater than 120 while [MgNC]/[MgCN] ≈ 22, so rearrangement must be the dominant pathway for the formation of MgCN in the IRC + 10216 stellar envelope. Petrie determined that if there is rapid interconversion of MgNC, which possesses a great deal of energy when formed because the

neutralization in the second step is highly exothermic, then the MgNC/MgCN ratio should be approximately 3.5. The larger observed ratio indicates that only about 15% of the reactions convert to MgCN in IRC + 10216.

In our system, laser ablation of the targets yields metastable metal atoms and cations, although we do not know if any cations reach the condensing matrix. A reaction mechanism similar to (1) and (2) above could account for a large MgNC/MgCN ratio in the matrix experiments. For beryllium, which ablates with a high fraction of energetic metastable species,[45−48] the following "$S_N2$" mechanism was shown to be very significant:[15]

$$\mathrm{Be^*} + \mathrm{NCH} \rightarrow [\mathrm{BeNCH}]^{\ddagger} \quad (3)$$

$$[\mathrm{BeNCH}]^{\ddagger} \rightarrow \mathrm{BeNC} + \mathrm{H} \quad (4)$$

Despite the propensity for Be* to insert into bonds,[33,45−48] far more BeNC than BeCN was formed on deposition of the matrix. A similar mechanism may well exist for the other alkaline earth metals and lead to the overwhelming favoritism of MNC products as opposed to MCN. If formed via metastable ablated atoms and not ions, no neutralization with its associated release of energy need occur. The energy released in reaction 4 above may not be sufficient to convert MNC to MCN. Ishii et al. calculated a barrier for this conversion to be 6.2 kcal $mol^{-1}$ for magnesium, which may be too great to overcome in the ablation and deposition process.[44] Insertion into the C−H bond, which leads to a small amount of BeCN in the beryllium experiments, may be a less viable option for the larger group 2 metals.

Another possibility for the failure to observe MCN absorptions is the apparently larger oscillator strengths for the C≡N bonds in MNC than for those in MCN. As Table 2 shows, DFT calculations predict a significant difference between the C≡N stretching intensities. Ishii et al. obtained an intensity ratio of 38:1 for this quantity.[44] Such a disparity in intensities could mask the observation of MgCN and other MCN products even if the concentration of this species were comparable to that of the MNC isomer.

The failure to observe MCN products may arise because of either low number density or small oscillator strengths of the C≡N stretching absorption. The former explanation seems more likely. Because observation of the Mg−N stretch of MgNC is well within the spectral capabilities of our instrument in the mid-IR, it should be possible to observe the Mg−C stretch of MgCN if produced in reasonably significant quantities. The HF and BP86 calculations both predict the intensities of these two modes to be comparable, and Petrie agrees.[43] While the 513.7 $cm^{-1}$ band in Figure 3a is certainly associated with the same product as the isocyanide band at 2076.1 $cm^{-1}$, on the basis of photolysis and annealing behavior, the band at 542.9 $cm^{-1}$ cannot denote a Mg−C stretch because such a vibrational mode should occur at a frequency *lower* than that of the Mg−N mode in MgNC. All of the reasonable calculated results in Table 4 support this conclusion and estimate a red shift of 55−80 $cm^{-1}$ for MgCN. Therefore, if there were an appreciable concentration of MgCN in the matrix, an observable MgCN stretch should lie in the spectra to the red of the clearly visible MgNC band in Figure 3. The lack of spectroscopic evidence for the other MCN products is caused by a low number density of these species on deposition. No evidence for MCN was observed in any of the far-infrared spectra.

## Conclusions

With the exception of the beryllium experiments,[15] in reactions of laser-ablated alkaline earth atoms with hydrogen cyanide, only monoisocyanides are produced in significant quantities. All of these isocyanides are linear with the band shapes becoming broader with increasing size of the group 2 metal atom, indicating a more "floppy" structure consistent with previous calculations.[7] As with previous studies of various cyanides and isocyanides in an argon matrix,[15,16,18] the C≡N stretching frequencies are between 2000 and 2100 $cm^{-1}$ with a carbon-13 isotopic shift of approximately 40 $cm^{-1}$. No MCN products were observed for the atoms heavier than beryllium as these would be characterized by C≡N frequencies above 2100 $cm^{-1}$ and larger isotopic shifts than in the isocyanides. Although the C≡N isotopic shifts in the isocyanides are virtually independent of the M atom, the value of these frequencies depend strongly on the mass of the group 2 atom, decreasing as M increases in size. The M-NC stretching modes were observed at 513.7, 403, and 338 $cm^{-1}$ for Mg, Ca, and Sr species, in agreement with DFT calculations.

This study represents the first vibrational infrared spectroscopy of the alkaline earth isocyanides, which have been studied with earnestness both experimentally and theoretically in the recent past. Because MgNC and MgCN were both observed in the stellar envelope of IRC + 10216, efforts to characterize group 2 cyanides have focused on these species. Despite several calculations on these products yielding a small energy difference between these two isomers, only the former is seen in this experiment. These results, as well as the difference in observed quantities in IRC + 10216, indicate that formation of these isomers does not take place in an equilibration process and instead favors the formation of MgNC with a seeming inability to cross the isomerization barrier. It is likely that the same situation occurs for the other alkaline earth reactions and is consistent with the mechanism previously proposed for beryllium−hydrogen cyanide reactions.

**Acknowledgment.** This work was supported by the Air Force Office of Scientific Research. Calculations were performed on the University of Virginia SP2 machine. Cambridge Isotope Laboratories generously provided the $K^{13}CN$.

## References and Notes

(1) Guélin, M.; Cernicharo, J.; Kahane, C.; Gomez-Gonzalez, J. *Astron. Astrophys.* **1986**, *157*, L17.
(2) Kawaguchi, K.; Kagi, E.; Hirano, T.; Takano, S.; Saito, S. *Astrophys. J.* **1993**, *406*, L39.
(3) Anderson, M. A.; Ziurys, L. M. *Chem. Phys. Lett.* **1994**, *231*, 164.
(4) Guélin, M.; Forestini, M.; Valiron, P.; Ziurys, L. M.; Anderson, M. A.; Cernicharo, J.; Kahane, C. *Astron. Astrophys.* **1995**, *297*, 183.
(5) Anderson, M. A.; Steimle, T. C.; Ziurys, L. M. *Astrophys. J.* **1994**, *429*, L41.
(6) Ziurys, L. M.; Apponi, A. J.; Guélin, M.; Cernicharo, J. *Astrophys. J.* **1995**, *445*, L47.
(7) Bauschlicher, C. W., Jr.; Langhoff, S. R.; Partridge, H. *Chem. Phys. Lett.* **1985**, *115*, 124.
(8) Kagi, E.; Kawaguchi, K.; Takano, S.; Hirano, T. *J. Chem. Phys.* **1996**, *104*, 1263.
(9) Pasternack, L.; Dagdigian, P. J. *J. Chem. Phys.* **1976**, *65*, 1320.
(10) Furio, N.; Dagdigian, P. J. *Chem. Phys. Lett.* **1985**, *115*, 358.
(11) Whitham, C. J.; Soep, B.; Visticot, J.-P.; Keller, A. *J. Chem. Phys.* **1990**, *93*, 991.
(12) Douay, M.; Bernath, P. F. *Chem. Phys. Lett.* **1990**, *174*, 230.
(13) Scurlock, C. T.; Steimle, T. C.; Suenram, R. D.; Lovas, F. J. *J. Chem. Phys.* **1994**, *100*, 3497.
(14) Scurlock, C. T.; Fletcher, D. A.; Steimle, T. C. *J. Chem. Phys.* **1994**, *101*, 7255.
(15) Lanzisera, D. V.; Andrews, L. *J. Am. Chem. Soc.* **1997**, *119*, 6292.
(16) Lanzisera, D. V.; Andrews, L.; Taylor, P. R. *J. Phys. Chem. A* **1997**, *101*, 7134.
(17) Martin, J. M. L.; Taylor, P. R. *J. Phys. Chem.* **1994**, *98*, 6105.
(18) Lanzisera, D. V.; Andrews, L. *J. Phys. Chem. A* **1997**, *101*, 9660.
(19) Lanzisera, D. V.; Andrews, L. *J. Phys. Chem. A* **1997**, *101*, 824.
(20) Bohn, R. B.; Andrews, L. *J. Phys. Chem.* **1989**, *93*, 3974.

(21) Frisch, M. J.; Trucks, G. W.; Schlegel, H. B.; Gill, P. M. W.; Johnson, B. G.; Robb, M. A.; Cheeseman, J. R.; Keith, T.; Petersson, G. A.; Montgomery, J. A.; Raghavachari, K.; Al-Laham, M. A.; Zakrzewski, V. G.; Ortiz, J. V.; Foresman, J. B.; Cioslowski, J.; Stefanov, B. B.; Nanayakkara, A.; Challacombe, M.; Peng, C. Y.; Ayala, P. Y.; Chen, W.; Wong, M. W.; Andres, J. L.; Replogle, E. S.; Gomperts, R.; Martin, R. L.; Fox, D. J.; Binkley, J. S.; Defrees, D. J.; Baker, J.; Stewart, J. P.; Head-Gordon, M.; Gonzalez, C.; Pople, J. A. *Gaussian 94*, Revision B.1; Gaussian, Inc.: Pittsburgh, PA, 1995.

(22) McLean, A. D.; Chandler, G. S. *J. Chem. Phys.* **1980**, *72*, 5639.

(23) Krishnan, R.; Binkley, J. S.; Seeger, R.; Pople, J. A. *J. Chem. Phys.* **1980**, *72*, 650.

(24) Hay, P. J.; Wadt, W. R. *J. Chem. Phys.* **1985**, *82*, 270.

(25) Wadt, W. R.; Hay, P. J. *J. Chem. Phys.* **1985**, *82*, 284.

(26) Hay, P. J.; Wadt, W. R. *J. Chem. Phys.* **1985**, *82*, 299.

(27) Becke, A. D. *Phys. Rev. A* **1988**, *38*, 3098.

(28) Perdew, J. P. *Phys. Rev. B* **1986**, *33*, 8822.

(29) Head-Gordon, M.; Pople, J. A.; Frisch, M. J. *Chem Phys. Lett.* **1988**, *153*, 503.

(30) Frisch, M. J.; Head-Gordon, M.; Pople, J. A. *Chem Phys. Lett.* **1990**, *166*, 275.

(31) Frisch, M. J.; Head-Gordon, M.; Pople, J. A. *Chem Phys. Lett.* **1990**, *166*, 281.

(32) Schlegel, H. B. *J. Comput. Chem.* **1982**, *3*, 214.

(33) Tague, T. J., Jr.; Andrews, L. *J. Am. Chem. Soc.* **1993**, *115*, 12111.

(34) Tague, T. J., Jr.; Andrews, L. *J. Phys. Chem.* **1994**, *98*, 8611.

(35) Andrews, L.; Willson, S. P.; Tague, T. J., Jr., unpublished results.

(36) Corlett, G. K.; Little, A. M.; Ellis, A. M. *Chem. Phys. Lett.* **1996**, *249*, 53.

(37) Thompson, C. A.; Andrews, L. *J. Am. Chem. Soc.* **1996**, *118*, 10242.

(38) Andrews, L.; Yustein, J. T. *J. Phys. Chem.* **1993**, *97*, 12700.

(39) Andrews, L.; Yustien, J. T.; Thompson, C. A.; Hunt, R. D. *J. Phys. Chem.* **1994**, *98*, 6514.

(40) Scott, A. P.; Radom, L. *J. Phys. Chem.* **1996**, *100*, 16502.

(41) Kapp, J.; Schleyer, P. v. R. *Inorg. Chem.* **1996**, *35*, 2247.

(42) Barrientos, C.; Largo, A. *J. Mol. Struct.: THEOCHEM* **1995**, *336*, 29.

(43) Petrie, S. *J. Chem. Soc., Faraday Trans.* **1996**, *92*, 1135.

(44) Ishii, K.; Hirano, T.; Nagashima, U.; Weis, B.; Yamashita, K. *J. Mol. Struct.: THEOCHEM* **1994**, *305*, 117.

(45) Thompson, C. A.; Andrews, L. *J. Am. Chem. Soc.* **1994**, *116*, 423.

(46) Thompson, C. A.; Andrews, L. *J. Chem. Phys.* **1994**, *100*, 8689.

(47) Andrews, L.; Chertihin, G. V.; Thompson, C. A.; Dillon, J.; Byrne, S.; Bauschlicher, C. W., Jr. *J. Phys. Chem.* **1996**, *100*, 10088.

(48) Thompson, C. A.; Andrews, L. *J. Phys. Chem.* **1996**, *100*, 12214.